

UC Berkeley

UC Berkeley Previously Published Works

Title

Al₂O₃ Surface Complexation for Photocatalytic Organic Transformations

Permalink

<https://escholarship.org/uc/item/0bf7k8rj>

Journal

Journal of the American Chemical Society, 139(1)

ISSN

0002-7863

Authors

Leow, Wan Ru
Ng, Wilson Kwok Hung
Peng, Tai
[et al.](#)

Publication Date

2017-01-11

DOI

10.1021/jacs.6b09934

Peer reviewed

This document is confidential and is proprietary to the American Chemical Society and its authors. Do not copy or disclose without written permission. If you have received this item in error, notify the sender and delete all copies.

Al₂O₃ Surface Complexation for Photocatalytic Organic Transformations

Journal:	<i>Journal of the American Chemical Society</i>
Manuscript ID	ja-2016-099349
Manuscript Type:	Article
Date Submitted by the Author:	21-Sep-2016
Complete List of Authors:	<p>Leow, Wan Ru; Nanyang Technological University, School of Materials Science and Engineering Ng, Wilson; Nanyang Technological University, Peng, Tai; Beijing Institute of Technology, School of chemistry Liu, Xinfeng; National Center for Nanoscience and Technology, Li, Bin; Nanyang Technological University, School of Materials Science and Engineering Shi, Wenxiong; Nanyang Technological University, School of Materials Science and Engineering Lum, Yanwei; UC Berkeley, ; E O Lawrence Berkeley National Laboratory, Joint Center for Artificial Photosynthesis, Materials Sciences Division Wang, Xiaotian; Nanyang Technological University, School of Materials Science and Engineering Lang, Xianjun; Central China Normal University, College of Chemistry Li, Shuzhou; Nanyang Technological University, School of Materials Science and Engineering Mathews, Nripan; Nanyang Technological University, Ager, Joel; Lawrence Berkeley National Laboratory, Materials Sciences Division Sum, Tze Chien; Nanyang Technological University, Division of Physics & Applied Physics, School of Physical & Mathematical Sciences Hirao, Hajime; Nanyang Technological University, Division of Chemistry & Biological Chemistry, School of Physical & Mathematical Sciences Chen, Xiaodong; Nanyang Technological University, School of Materials Science and Engineering</p>

SCHOLARONE™
Manuscripts

Al₂O₃ Surface Complexation for Photocatalytic Organic Transformations

Wan Ru Leow,[†] Wilson Kwok Hung Ng,[‡] Tai Peng,[†] Xinfeng Liu,[‡] Bin Li,[†] Wenxiong Shi,[†] Yanwei Lum,^{§,||} Xiaotian Wang,[†] Xianjun Lang,[†] Shuzhou Li,[†] Nripan Mathews,[†] Joel W. Ager,^{§,||} Tze Chien Sum,[‡] Hajime Hirao,^{*,‡} and Xiaodong Chen^{*,†}

[†]School of Materials Science and Engineering, Nanyang Technological University, 50 Nanyang Avenue, Singapore 639798.

[‡]School of Physical and Mathematical Sciences, Nanyang Technological University, 21 Nanyang Link, Singapore 637371.

[§]Joint Center for Artificial Photosynthesis, Materials Sciences Division, Lawrence Berkeley National Laboratory, California 94720, United States.

^{||}Department of Materials Science and Engineering, University of California, Berkeley, California 94720, United States.

KEYWORDS: Photocatalysis; Al₂O₃; surface complex; benzylalcohol oxidation

ABSTRACT: The use of sunlight to drive organic reactions constitutes a green and sustainable strategy for organic synthesis. Herein, we discovered that the earth-abundant aluminum oxide (Al₂O₃), though paradigmatically known to be an insulator, could induce an immense increase in the selective photo-oxidation of different benzyl alcohols in the presence of a large variety of dyes and O₂. This unique phenomenon is based on the surface complexation of benzyl alcohol (BnOH) with the Brønsted base sites on Al₂O₃, which reduces its oxidation potential and causes an upshift in its HOMO for electron abstraction by the dye. The surface complexation of O₂ with Al₂O₃ also activates the adsorbed O₂ for receiving electrons from the photoexcited dyes. This discovery brings forth a new understanding on utilizing surface complexation mechanisms between the reactants and earth abundant materials to effectively achieve a wider range of photoredox reactions.

1. INTRODUCTION

Photoredox catalysis has great potential in facilitating organic transformations to valuable products,^{1,2} as it is environmentally-friendly, cost-effective, and easily realized by mere household fixtures. Therefore much research has been conducted on photo-absorbing molecules and complexes to convert solar energy to chemical energy.³ Out of these, Ru-based polypyridyl complexes have attracted immense popularity due to their ease of synthesis, stability, and good photoredox capabilities.^{4,5} Recently, the merging of photocatalysis and other types of catalysis e.g., organocatalysis^{6,7} and nickel^{8,9} or gold^{10,11} catalysis, could enable a large variety of difficult organic transformations^{1,12,13} such as the coupling of aryl halides with amino acids,⁸ tertiary anilines,^{14,15} carboxylic acids,¹⁶ organoborates,^{9,17,18} and α -oxo acids.¹⁹ Meanwhile, selective oxidation constitutes a class of difficult organic transformation, e.g. the oxidation of benzyl alcohols to aldehydes²⁰⁻²³ and sulfides to sulfoxides,^{24,25} which is essential for converting raw materials into fine chemicals especially in the flavor and fragrance industry.^{20,24,26} The typical synthesis route requires toxic oxidants that are detrimental to health and the environment.²⁷⁻³⁰ As for the photocatalytic redox route, the reaction can proceed only if the redox potential of the photocatalyst is greater than that of the reactants³. Conventional strategies to fulfill this condition include using wide band gap semiconductors³¹ such as TiO₂^{20,24} or Nb₂O₅³², and modifying the cation^{3,33,34} or ligands of transition metal complexes to tune the redox potential.^{3,35} However, the former method can only utilize the short wavelength range of the solar spectrum, while the latter requires unique photocatalysts to be synthesized for specific reactions.

In the past development of photocatalysis, aluminum oxide (Al₂O₃) has played a supporting rather than a central role, serving as high surface area supports and photochemically inert barriers.^{36,37} This is because alumina is an electrical insulator with a wide band gap of 8.7 eV.³⁸ However, Al₂O₃, in particular the γ -phase, possesses unique surface properties such as bifunctional Brønsted and Lewis acid and base sites,^{39,40} which can endow supported materials with catalytic activity that is absent in the pristine materials.^{41,42} Examples include Ag/Al₂O₃ for enhanced NO reduction^{43,44} and V₂O₅/Al₂O₃ for the photo-oxidation of cyclohexane.⁴⁵ Thus we propose that the redox potentials of organic reactants can be modified through surface complexation with Al₂O₃, which can be coupled with photocatalysis to facilitate demanding organic transformations under mild conditions.

In this article, we report that Al₂O₃ surface complexation can enable the highly selective oxidation of benzyl alcohols to benzaldehydes in the presence of dye, O₂ and visible light, even though negligible oxidation occurred with the dye alone. This phenomenon can be extended to dyes of different moieties. The underlying mechanism is that the oxidation potential of benzyl alcohol may be decreased through simple complexation with Al₂O₃, thus rendering it susceptible to oxidation by photocatalysts with smaller redox potentials. The complexation of O₂ with Al₂O₃ also enables it to receive electrons from the photoexcited dye, thus facilitating the overall transfer of protons and electrons from benzyl alcohol to O₂. This method would bring forth the potential of utilizing surface complexation mechanisms between the reactants and earth abundant materials to achieve a wider range of photoredox reactions.

2. MATERIALS AND METHODS

2.1 Preparation and Characterization of Al₂O₃

All solid catalysts were purchased from Sigma Aldrich and Alfa Aesar and used without further modification. The synthesized Al₂O₃ was prepared by solid state reaction, in which 7.5 g of aluminum nitrate nonahydrate (Al(NO₃)₃·9H₂O) dissolved in 50 ml deionized water was adjusted to pH 7.0 with NH₃·H₂O solution, dried, and then calcined at 600 °C.

Powder X-ray diffraction (XRD) was recorded by a Bruker-AXS X-ray diffractometer with Cu K α irradiation ($\lambda = 1.5418$ Å). The morphologies of the samples were examined by scanning (SEM, JEOL-JSM-7600F) and high-resolution transmission electron microscopy (HRTEM, JEOL-JEM-2100F). The Brunauer–Emmett–Teller (BET) surface area was measured with an ASAP 2020 apparatus (Micromeritics Instrument Corp.). UV-visible diffuse reflectance spectroscopy was used to measure the optical properties of Al₂O₃ with barium sulfate as the reference and transformed to the absorption spectra according to the Kubelka-Munk relationship. The CO₂-TPD was performed on the Auto Chem 2920 (USA) apparatus. 0.10 g of the sample was loaded in a U-shaped quartz tube, heated at 550 °C for 1 h in helium flow and then cooled to 40 °C, in order to saturate the sample with CO₂. The CO₂-TPD spectrum was then measured in the temperature range of 40–600 °C at a constant heating rate of 10 °C min⁻¹.

2.2 Reaction and Post-Reaction Analysis

All reactants and catalysts were purchased from Sigma Aldrich and used without further purification, while all solvents were purchased from Fisher Chemical. The solid catalysts were thermally pre-treated at 200 °C prior to reaction to remove surface water and impurities. In a typical reaction, 50 mg of Al₂O₃, 0.5 μ mol of Ru(bpy)₃Cl₂, and 0.1 mmol of BnOH were added to 5 mL of CH₃CN in a Pyrex vessel, and allowed to stir for 30 min in the dark. O₂ was then purged into the Pyrex vessel to achieve an O₂ atmosphere of pressure 0.1 MPa. The reaction mixture was then illuminated by the 7 W white light household LED, the irradiating wavelength range of which was measured to be 400-700 nm, with two maxima at 450 and 550 nm (Figure S8a), under magnetic stirring at 800 rpm.

Upon reaction completion, Al₂O₃ was separated from the reaction mixture by centrifugation. The product identities were confirmed by comparison of the gas chromatography (GC) retention times with that of standard samples. The products were then quantitatively analyzed through a GC (Agilent 7890A) equipped with a flame ionization detector (FID) and Agilent Technology 19091J-413 capillary column (30 m \times 0.32 mm \times 0.25 mm) using high-purity N₂ as the carrier gas and chlorobenzene as the internal standard. The standard analysis conditions are: injector temperature 250 °C, detector temperature 300 °C, column temperature ramped from 50 °C to 300 °C with a rate of 20 °C min⁻¹. GC–MS analysis was conducted with a Shimadzu GC 2010 gas chromatograph equipped with a Shimadzu GCMSQP2010 Ultra mass spectrometer and a Restek (Rxi®-5Sil MS) capillary column (30 m \times 0.25 mm \times 0.25 mm), coupled with an electron ionization mass spectrometer with high-purity He as the carrier gas.

2.3 Cyclic Voltammetry

The Al₂O₃ modified electrode was fabricated according to procedures present in literature. Basically, Al₂O₃ paste was deposited using the doctor-blade technique on fluorine-doped stannic oxide coated glass (sheet resistance of 15 Ω /sq., Nippon Sheet Glass Co., Ltd., Japan). The resultant layer was dried in air at room temperature and heated at 450 °C for 1 hour before cooling to room temperature. Cyclic voltammetry was carried out using a CHI 660D electrochemical workstation (CH Instruments, Inc., Austin, USA). A three-electrode configuration was used for the measurement of cyclic voltammetry: the Al₂O₃ modified FTO glass functions as the working electrode, a Pt wire as the counter electrode, and an Ag/Ag⁺ electrode as the reference. A 0.1 M solution of tetrabutylammonium hexafluorophosphate (TBAPF₆) in CH₃CN was used as the supporting electrolyte. Ferrocene was employed as internal standard. A glassy carbon electrode was used as working electrode for the measurement of oxidative potential of BnOH.

2.4 Theoretical Simulation of the BnO–Al₂O₃ Surface Complex and Dyes' Energy Structure

All calculations are based on the Al₂O₃ model proposed by Digne et al.⁴⁶. A slab with the (110) facet exposed and dimensions of (16.826Å*16.136Å*25.000Å) is created to model the BnOH adsorption, the Periodic boundary condition calculations were conducted with VASP computational packages.⁴⁷⁻⁵⁰ The PBE functional and PAW method were used for calculation and only the Γ point is chosen for Brillouin zone sampling.⁵¹⁻⁵³ An isolated complex was used to describe the BnO–Al₂O₃ surface complex approximately; it was assumed that neighbouring BnOH, Ru(bpy)₃²⁺ and solvent molecules do not exert a large influence on its energy levels. The HOMO level of the free BnOH molecule is determined from the vertical ionization energy, which is calculated by the Gaussian09 package using the PBE functional with 6-31+G* basis set. The vacuum level is used to locate the absolute energy level.

The Gaussian09 package was used for the DFT calculation of the dye molecules. The B3LYP functional with 6-31G* basis set is used for the calculations. For Rose Bengal, the iodide atoms were treated with the SDD basis set. To take the solvation effect into account, the self-consistent reaction field (SCRF) approach was used and the solvent involved is acetonitrile.⁵¹⁻⁵³ The energy level of Rhodamine B in vacuum is very low due to its positive charge (no counter ion is added to the system). The HOMO-LUMO gaps are almost always larger than the S₀S₁ transition energy predicted by TDDFT. This is the most significant for Ru(bpy)₃²⁺ as it is cationic and its electronic transition is MLCT, which tends to deviate a lot from its HOMO-LUMO gap.

2.5 Time-Resolved Photoluminescence (TRPL)

A pump wavelength of 400 nm was used for the TRPL measurements, which originates from the frequency doubled 800 nm laser pulses generated from a Coherent Libra™ Regenerative Amplifier using a Beta Barium Borate (BBO) crystal. The luminescence signal was collected and then dispersed by a DK240 1/4-m monochromator with 300 g mm⁻¹ grating. The transient photoluminescence signal was resolved by an Optronis Optoscope™ streak camera system, which possesses an ultimate temporal resolution of about 10 ps when operated at the fastest scan speed.

3. RESULTS AND DISCUSSION

First of all, a series of different benzyl alcohols **1a-k** was tested with $\text{Ru}(\text{bpy})_3^{2+}$ as the photosensitizer and mild conditions such as irradiation with a 7 W household white light LED and O_2 as the oxidant (Figure 1a). The Al_2O_3 used is the commercially-available Aldrich 517747, unless otherwise stated. XRD studies showed that the Al_2O_3 is γ -crystalline (Figure S1a), while HRTEM and SEM revealed that the Al_2O_3 comprises micron-sized particles made up of an aggregation of nano-rod structures (Figures S2a and S3a). The Al_2O_3 also boasts a mesoporous structure and large BET surface area of $332 \text{ m}^2/\text{g}$, which are favorable for catalysis (Figure S4a and Table S1). It can be seen from Figure 1b that the simple addition of Al_2O_3 caused a large increase in conversions for all 11 benzyl alcohols (52.5-88.6%, with most over 75.0%), while $\text{Ru}(\text{bpy})_3^{2+}$ alone only afforded trace conversions (<5.0%). The addition of Al_2O_3 has increased the turnover number (TON) of benzyl alcohol (BnOH) with respect to $\text{Ru}(\text{bpy})_3^{2+}$ by over 30 times (Figure S5a). This discovery is paradoxical to existing paradigms as Al_2O_3 is known as an insulator³⁸ and tends to play a supporting rather than a central role in photocatalysis.^{36,37}

The addition of Al_2O_3 to $\text{Ru}(\text{bpy})_3^{2+}$ could also significantly improve the selective oxidation of phenol **2a** to cyclohexa-2,5-dien-1-one **2'a** (from 0 % to 14.5 %) and hydroquinone **2b** to quinone **2'b** (from 21.0 % to 61.3 %), but led to only a small improvement for aliphatic alcohols such as butanol **2c**, pentanol **2d** and cyclohexanol **2e** (from 0.130-0.243 % to 4.88-8.42 %, Table S2). For furfuryl alcohol **2f**, although the conversion was 99.3 %, there was no selectivity for furfural **2'f** (Table S2). The combined Al_2O_3 - $\text{Ru}(\text{bpy})_3^{2+}$ surface complex system also showed improved conversion in the hydroxylation of phenylboronic acid **3a** to phenol **3'a** (from 14.6 % to 96.0 %), but not the epoxidation of styrene **3b** (Table S3). The oxidation of benzylamine **3c** and thioanisole **3d** to imine **3'c** and sulfoxide **3'd** were easily able to proceed to completion with $\text{Ru}(\text{bpy})_3^{2+}$ only, hence the addition of Al_2O_3 would not be necessary. Due to the limited scope of the article, only the mechanism of BnOH oxidation would be examined in detail.

It is interesting that the phenomenon appears to be exclusive to Al_2O_3 ; with other metal oxides such as SiO_2 and MgO , negligible BnOH conversions were observed (Figure 1c). The TON achieved with Al_2O_3 was >50 times higher than that with SiO_2 and MgO (Figure S5a). The initial rate of conversion, turnover frequency (TOF) and quantum yield were relatively high with Al_2O_3 , but decreased due to the decreasing concentration of BnOH available for reaction and the formation of hydroxyl groups on the Al_2O_3 surface⁴⁰ when the byproduct H_2O_2 ⁵⁴⁻⁵⁶ decomposes to H_2O (Figure S5b-c and S6).⁵⁷ Control studies revealed that negligible BnOH conversion occurred in the dark and under N_2 (Figure S7a), which indicated that (1) the reaction proceeds via a photocatalytic pathway, and (2) O_2 is essential for the transformation of BnOH, suggesting that O_2 serves as a sacrificial electron acceptor that receives 2 electrons and 2 protons from BnOH to form benzaldehyde. The BnOH conversion generally increased with the amount of Al_2O_3 used, but the extent of increment becomes less significant for larger amounts of Al_2O_3 (Figure S7b). Figure 1d showed that the phenomenon also applies to other commercial Al_2O_3 and Al_2O_3 synthesized via solid state reaction, but not for the non-mesoporous commercial Al_2O_3 [Aldrich 718475]. It can also be observed that the basic Al_2O_3 [Alfa Aesar

11503] showed higher conversion compared to the neutral [Alfa Aesar 11502] and acidic Al_2O_3 [Alfa Aesar 11501], which suggests the importance of Brønsted basicity in enabling the reaction. The characterizations of the aforementioned Al_2O_3 samples can be found in Figures S1-4 and Table S1.

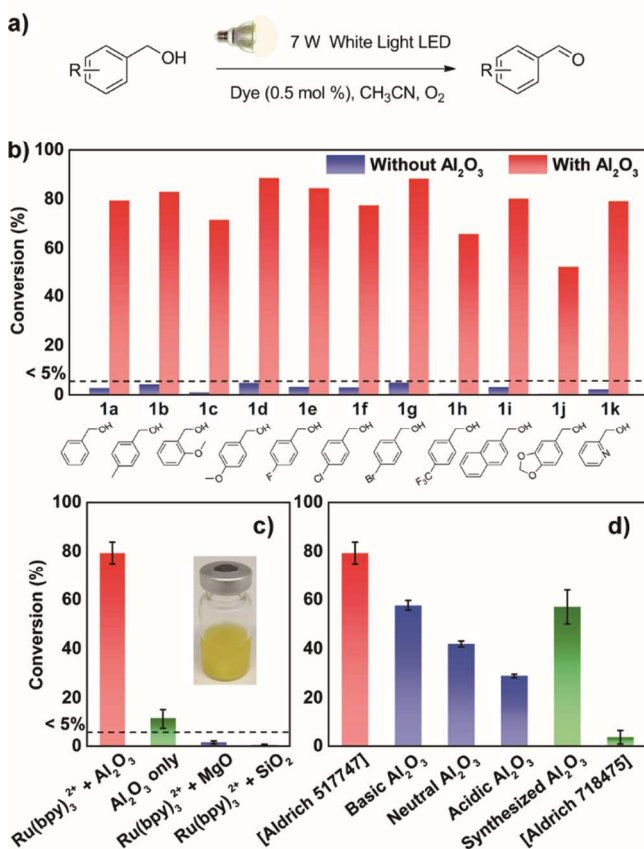


Figure 1. Photocatalytic organic transformation catalyzed by the Al_2O_3 and dye surface complex system. a) Visible light driven oxidation of benzyl alcohol to aldehyde with O_2 . b) Conversion of different benzyl alcohols by $\text{Ru}(\text{bpy})_3^{2+}$ with and without Al_2O_3 . c) Conversion of BnOH with different metal oxides and $\text{Ru}(\text{bpy})_3^{2+}$. d) Extensiveness of the Al_2O_3 and $\text{Ru}(\text{bpy})_3^{2+}$ dual surface complex system towards different commercial Al_2O_3 products.

This phenomenon can also be extended to a large variety of dyes with different moieties, i.e. naphthalene, anthracene, porphyrin, and perylene. While none of the dyes were able to oxidize BnOH in the absence of Al_2O_3 , most were able to achieve some BnOH conversion when Al_2O_3 was added (Figure 2). A positive relationship can be observed between the dye excitation wavelengths (Figure S8d) and extent of BnOH conversion. $\text{Ru}(\text{bpy})_3^{2+}$ and perylene-3,4,9,10-tetracarboxylic dianhydride (PTCDA), with excitation wavelengths between 450 and 550 nm, showed extremely high conversions of $79.4(\pm 4.4)\%$ and $82.2(\pm 11.1)\%$, respectively. Commercial dyes such as Rose Bengal and Rhodamine B were also able to effect significant conversions of $64.5(\pm 4.6)\%$ and $36.2(\pm 2.6)\%$, respectively, but their lack of stability undermined their photocatalytic activity. 9-anthracenecarboxylic acid (ACA) and 1,4,5,8-naphthalenetetracarboxylic dianhydride (NTCDA), with absorbance peaks in the range of 300–400 nm that is far from the LED wavelengths, yielded a low conversion of $23.0(\pm 1.7)\%$ and $13.1(\pm 5.3)\%$, respectively. However, when the light source was switched to one with a

wavelength range that is suitable for absorption by the ACA (350-750 nm), the combined Al₂O₃-ACA surface complex system was able to effect a significant degree of conversion, i.e. 78.0% in 2 h (Figure S9a). It must be noted that ACA by itself was only able to achieve a low conversion of 27.3%. This suggests that different wavelengths of light can be accessed by the Al₂O₃-dye surface complex system by merely selecting a dye with an appropriate excitation wavelength. For instance, the use of Ru(bpy)₃²⁺ with Al₂O₃ showed higher conversion than Degussa P25 under the 450-750 nm wavelength range, and the use of PTCDA with Al₂O₃ showed higher conversion under the 490-750 nm wavelength range (Figure S9b).

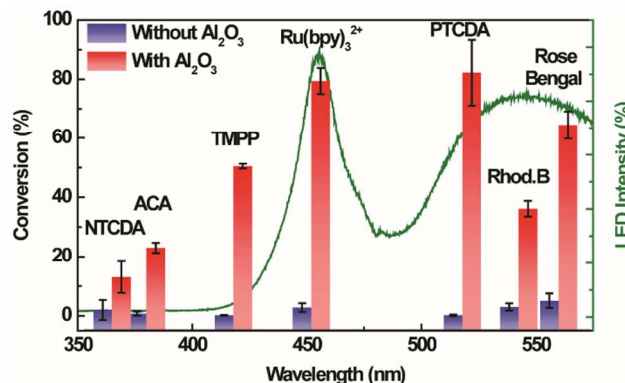


Figure 2. The extensiveness of the Al₂O₃ and dye surface complex system towards dyes of different moieties.

3.1 Decrease of BnOH Oxidation Potential due to Benzylic O-H dissociation

The success of the Al₂O₃-Ru(bpy)₃²⁺ photocatalytic system and the negligible activity of the individual Ru(bpy)₃²⁺ can be explained by the decrease of the BnOH oxidation potential through surface complexation with Al₂O₃. In Figure 1b, 2-methoxybenzyl alcohol **1c** (71.6%) showed a lower conversion relative to 4-methoxybenzyl alcohol **1d** (88.6%) (Figure 1b), as the methoxy group in the ortho position provides greater steric hindrance around the O-H group. The decrease in conversion with increasing amounts of acetic acid added (Figure S10a) suggests that the Brønsted base sites on Al₂O₃ (Figures S11a-b) are responsible for the surface complexation, as acetic acid would compete with BnOH for chemisorption on Brønsted base sites. Cyclic voltammetry conducted on BnOH in acetonitrile with a bare glassy carbon electrode showed an irreversible BnOH oxidation peak at around +2.0 V vs Ag/AgCl³⁵. As the Ru(bpy)₃²⁺/Ru(bpy)₃³⁺ potential in acetonitrile is +1.29 V vs SCE,^{3,13} BnOH cannot be oxidized by Ru(bpy)₃³⁺. However, the use of an Al₂O₃-modified electrode resulted in an additional oxidation feature at around +0.63 V vs Ag/AgCl (Figure 3a), which is within the oxidative potential of Ru(bpy)₃³⁺. This oxidation feature is suggestive of a chemisorbed BnO-Al₂O₃ surface complex, which is oxidized at the Al₂O₃-bare electrode interface. The BnO-Al₂O₃ surface complex is characterized by a lower oxidation potential and can be easily oxidized by Ru(bpy)₃³⁺ (Figure 4, step II). No additional oxidation feature was detected for the SiO₂- and MgO-modified electrodes (Figure S13a), while similar oxidation peaks are detected for other BnOH derivatives (Figure S13b-d). The addition of acetic acid caused a quenching of the oxidation feature at +0.63 V vs Ag/AgCl (Figure 3a), indicating that the BnO-Al₂O₃ surface complexation occurs through O-H de-protonation by the Brønsted base surface sites. **As**

little BnOH conversion occurred when Al₂O₃ was replaced by inorganic bases (Figure S10b), this suggests that surface complexation on Al₂O₃ has a stabilizing effect on the deprotonated BnO⁻.

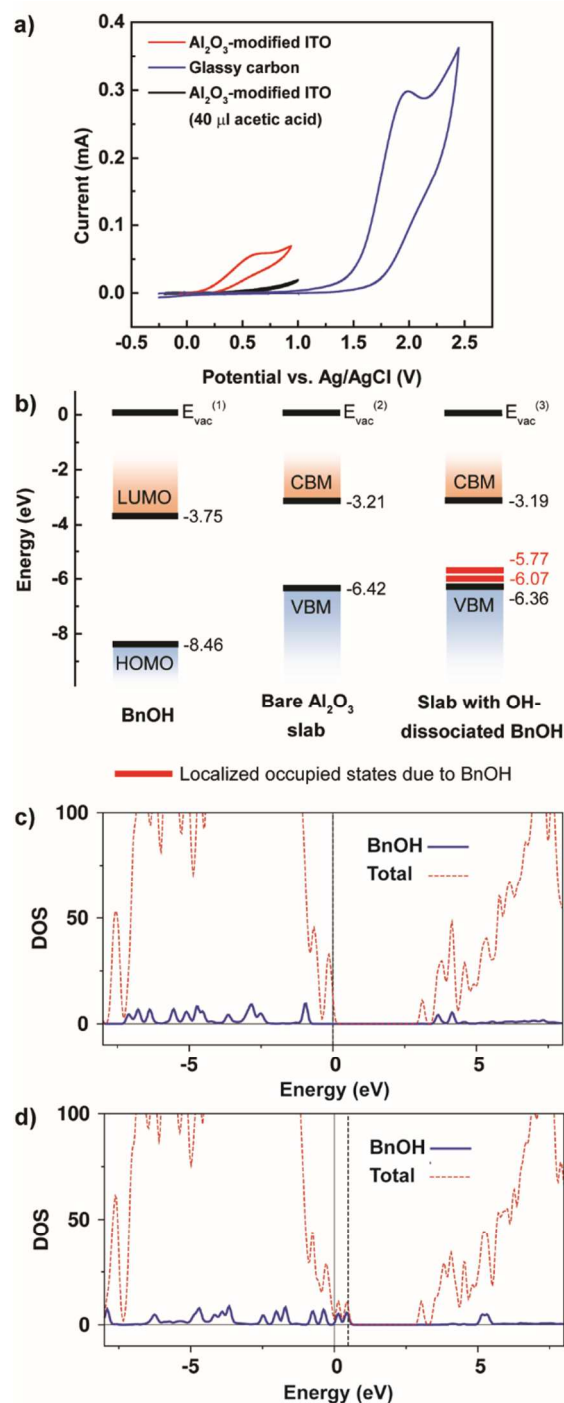


Figure 3. Chemisorption on the surface of Al₂O₃ decreases the oxidation potential of BnOH. a) Cyclic voltammogram of BnOH with Al₂O₃-modified (red) and bare electrodes (blue), and 40 μl acetic acid (black). b) Energy levels of Al₂O₃, free BnOH and the chemisorbed surface complex. c) DOS of BnOH physically adsorbed to the Al_{III} site, and d) chemisorbed via OH dissociation. The dashed line indicates the formation of localized occupied states just above the VBM of Al₂O₃.

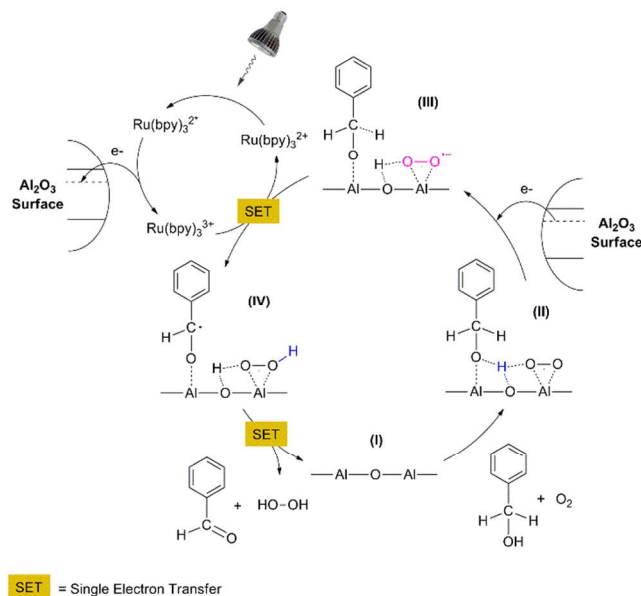


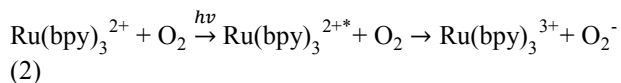
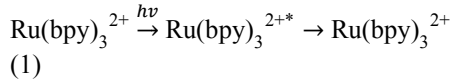
Figure 4. Proposed mechanism of visible-light-driven BnOH oxidation by the Al_2O_3 and $\text{Ru}(\text{bpy})_3^{2+}$ surface complex system.

Furthermore, the decrease of BnOH oxidation through surface complexation is validated through first-principles calculations on free BnOH and BnOH adsorbed on the most widely exposed plane of the γ -phase Al_2O_3 surface, the (110) facet, based on the Digne model (Figure S14a)⁴⁶. The HOMO of the free BnOH molecule was calculated as -8.46 eV (Figure 3b). The DOS diagrams for the adsorption of BnOH onto the Al_{III} site (Figure 3c and d) show that O-H dissociation results in an upward shift in the PDOS of BnOH and the appearance of two additional occupied peaks (the left-hand side of the black dashed line with energy > 0 eV). The two peaks correspond to occupied localized states arising from the molecule (Figure S14d), and their energy levels are colored in red in Figure 3b. These occupied states arise as BnOH draws electron density from the surface after O-H dissociation to stabilize its new alkoxide state, which causes it to become electron rich while creating an electron deficiency in a localized area of the surface. The electron gain by BnOH increases the electron repulsion within the molecule and causes an upward shift in energy level. As the C-H σ -bonds are located at the valence edge, a hole generated on the surface by $\text{Ru}(\text{bpy})_3^{3+}$ oxidation and transferred to BnOH would result in the weakening and subsequent cleavage of the C-H bond to form benzaldehyde (Figure 4, steps III-IV). In this way, Al_2O_3 enables the oxidation of BnOH through the formation of a chemisorbed surface complex that has a lower oxidation potential than that of $\text{Ru}(\text{bpy})_3^{2+}/\text{Ru}(\text{bpy})_3^{3+}$.

3.2 Electron Transfer from $\text{Ru}(\text{bpy})_3^{2+}$ due to Activation of O_2

As a control experiment to confirm the interaction between Al_2O_3 and the photosensitizer, we grafted $\text{Ru}(\text{bpy})_3^{2+}$ to the surface of Al_2O_3 through $-\text{COOH}$ groups, in order to reduce the proximity between the two (Table S4, Column [b]). As BnOH conversion is generally greater for the grafted $\text{Ru}(\text{bpy})_3^{2+}$ relative to the ungrafted $\text{Ru}(\text{bpy})_3^{2+}$, the interaction of the dye with Al_2O_3 appears to be significant for the reaction. To understand the nature of such an interaction, time-resolved photoluminescence (TRPL) spectroscopy was used to study

the charge-transfer dynamics between the ungrafted $\text{Ru}(\text{bpy})_3^{2+}$ and Al_2O_3 . Firstly, $\text{Ru}(\text{bpy})_3^{2+}$ was photoexcited using 400 nm laser pulses. The excited species $\text{Ru}(\text{bpy})_3^{2+*}$ are generated from the metal-to-ligand charge transfer (MLCT) process⁵⁸ and decay exponentially with time, yielding the resultant TRPL signal (Figure 5a). This PL decay arises from a combination of radiative and non-radiative processes: (1) the recombination of charge carriers to regenerate $\text{Ru}(\text{bpy})_3^{2+}$; and (2) the loss of an electron to O_2 through electron transfer.



As a similar TRPL lifetime can be observed in the absence of O_2 (Figure 5b and Table 1), the recombination pathway (1) appears to be the dominant process. Although the oxidation potential of O_2 is suitable for receiving electrons from $\text{Ru}(\text{bpy})_3^{2+*}$, there appears to be little electron transfer between $\text{Ru}(\text{bpy})_3^{2+*}$ and O_2 within the 300 ns timeframe in the case of $\text{Ru}(\text{bpy})_3^{2+}$ alone. The lack of BnOH conversion with MgO and SiO_2 may also be due to negligible electron transfer from $\text{Ru}(\text{bpy})_3^{2+*}$ to MgO or SiO_2 , as the lifetimes of $\text{Ru}(\text{bpy})_3^{2+*}$ on MgO and SiO_2 are largely similar to that of $\text{Ru}(\text{bpy})_3^{2+*}$ alone (Figure 5a and Table 1). There also appears to be no electron transfer between $\text{Ru}(\text{bpy})_3^{2+*}$ and BnOH, as no change in the lifetime of $\text{Ru}(\text{bpy})_3^{2+*}$ was observed when BnOH was added (Figure S15).

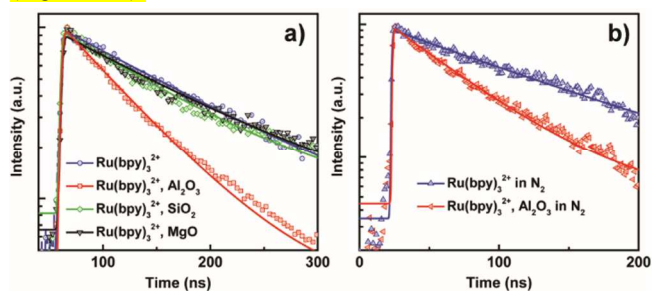


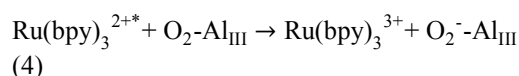
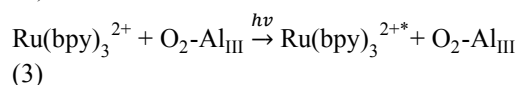
Figure 5. Decay kinetics of TRPL signals of $\text{Ru}(\text{bpy})_3^{2+}$ and $\text{Ru}(\text{bpy})_3^{2+}$ adsorbed on Al_2O_3 , SiO_2 , and MgO under a) ambient and b) N_2 atmosphere.

Table 1. Decay lifetimes of the samples measured under ambient and N_2 atmospheres.

Entry	Sample	Atmosphere	Lifetime (ns)
1	$\text{Ru}(\text{bpy})_3^{2+}$	Ambient	125 ± 2
2	$\text{Ru}(\text{bpy})_3^{2+} + \text{Al}_2\text{O}_3$	Ambient	63 ± 1
3	$\text{Ru}(\text{bpy})_3^{2+} + \text{SiO}_2$	Ambient	105 ± 2
4	$\text{Ru}(\text{bpy})_3^{2+} + \text{MgO}$	Ambient	122 ± 2
5	$\text{Ru}(\text{bpy})_3^{2+}$	N_2	115 ± 2
6	$\text{Ru}(\text{bpy})_3^{2+} + \text{Al}_2\text{O}_3$	N_2	55 ± 1

Finally, we examine the case where $\text{Ru}(\text{bpy})_3^{2+}$ is adsorbed on Al_2O_3 . It can be seen that under both ambient and nitrogen conditions, the lifetime of $\text{Ru}(\text{bpy})_3^{2+*}$ in the presence of Al_2O_3 is almost half that of $\text{Ru}(\text{bpy})_3^{2+*}$ alone. This suggests that in

addition to the aforementioned recombination process, there is also a dominant electron transfer process from $\text{Ru}(\text{bpy})_3^{2+*}$ to form $\text{Ru}(\text{bpy})_3^{3+}$. The idea that an additive or co-catalyst can render a reaction thermodynamically feasible by accepting and transferring electrons has been frequently proposed in literature.⁵⁹⁻⁶¹ However, DFT calculations reveal that the CBM of the Al_2O_3 surface is too high at -3.21 eV to receive an electron from $\text{Ru}(\text{bpy})_3^{2+*}$. Hence, it is hypothesized that electron transfer may not have occurred directly from $\text{Ru}(\text{bpy})_3^{2+*}$ to Al_2O_3 , but to a O_2 molecule strongly complexed to the surface of Al_2O_3 , which may not have been released in the nitrogen atmosphere (Figure 6a). This hypothesis is consistent with a previous report that O_2 may play a crucial role in the electron transfer processes of organic adsorbates at the Al_2O_3 surface.⁶² DFT calculations show that in the gas phase of O_2 , the π_x and π_y are half occupied and have the same energy level. However, when O_2 strongly complexed with the Al_{III} site of Al_2O_3 , the π_x and π_y become energetically inequivalent and lead to a singly occupied π orbital on the surface. This results in the appearance of a localized vacant band at -5.07 eV (Figure 6b and c), which is suitable for accepting electrons from $\text{Ru}(\text{bpy})_3^{2+*}$ to yield superoxide O_2^- (Equations 3-4 and Figure 4, steps II-III).



The loss of electrons from $\text{Ru}(\text{bpy})_3^{2+*}$ would then yield the oxidant species $\text{Ru}(\text{bpy})_3^{3+}$, which would drive the reaction forward by removing an electron from the adsorbed BnOH to form an α -carbon radical (Figure 4, steps III-IV). The overall process is such that, with Al_2O_3 and the photoexcited $\text{Ru}(\text{bpy})_3^{2+*}$ acting in tandem as a shuttle, an electron transfer is enabled from BnOH to O_2 . It should be noted that the localized vacant band of the $\text{O}_2\text{-Al}_{\text{III}}$ complex at -5.07 eV is also suitable for accepting electrons from the excited states of all dyes used in Figure 2 (Figure S16a), which could account for the efficacy of the Al_2O_3 -dye surface complex system.

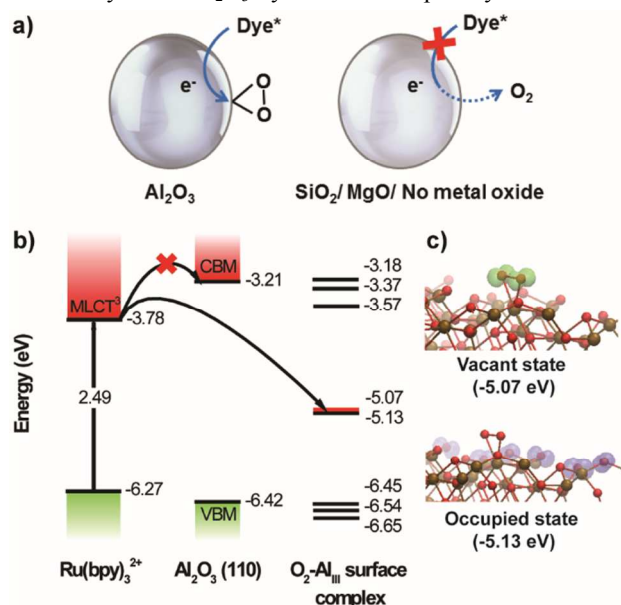


Figure 6. a) Scheme of proposed electron transfer between dye and O_2 . b) Occupied and vacant states of the singly occupied $\text{O}_2\text{-Al}_{\text{III}}$ surface complex. c) Energy levels of $\text{Ru}(\text{bpy})_3^{2+}$, Al_2O_3 , and O_2 .

ried π orbital which arose due to O_2 and Al_2O_3 surface complexation. c) Energy levels of $\text{Ru}(\text{bpy})_3^{2+}$, Al_2O_3 , and O_2 .

4. CONCLUSION

In conclusion, we employed the unconventional strategy of utilizing Al_2O_3 surface complexation to modify the oxidation potential of organic reactants, which would enable the oxidation of organic reactants with high oxidation potentials inaccessible to the unassisted photocatalyst. This has been successfully demonstrated through the photocatalytic oxidation of benzyl alcohols to benzaldehydes. High conversion and selectivity can be achieved with the surface complex systems comprising Al_2O_3 and a variety of dyes, but not with these dyes alone. The formation of the chemisorbed $\text{BnO-Al}_2\text{O}_3$ surface complex is attributed to the strong Brønsted base sites on Al_2O_3 , which accepts protons from benzylic O-H. This causes a shift in the oxidation potential of BnOH , which enhances the ease of subsequent electron and C-H proton abstraction to form benzaldehyde. The surface complexation of O_2 with Al_2O_3 also activates the adsorbed O_2 for receiving electrons from the photoexcited dyes. This discovery may subvert our understanding of the role of Al_2O_3 in photocatalytic reactions. For instance, it may be possible for Al_2O_3 to play a role beyond that of a mere support or scaffold in the performance enhancement in solar hydrogen production⁶³ and dye-sensitized solar cells.^{64,65} This discovery brings forth a new methodology of utilizing surface complexation mechanisms between the reactants and earth-abundant materials to effectively achieve a wider range of photoredox reactions.

ASSOCIATED CONTENT

Supporting Information

Experimental procedures, control experiments, DFT calculations, material surface characterizations and the reaction mechanism are included in the supporting information.

AUTHOR INFORMATION

Corresponding Authors

*chenxd@ntu.edu.sg (X.C.)

*hirao@ntu.edu.sg (H.H.)

Author Contributions

The manuscript was written through contributions of all authors. All authors have given approval to the final version of the manuscript.

Notes

The authors declare no competing financial interests.

ACKNOWLEDGMENT

We gratefully acknowledge financial support from Singapore Ministry of Education Tier 1 (RG130/14) and the Singapore NRF through the Singapore-Berkeley Research Initiative for Sustainable Energy (SinBeRISE) CREATE Programme. T.C.S. acknowledges the financial support from Singapore Ministry of Education Tier 2 (MOE2013-T2-1-081 and MOE2014-T2-1-044). H.H. is grateful for a Nanyang Assistant Professorship.

REFERENCES

- (1) Devery III, J. J.; Stephenson, C. R. J. *Nature* **2015**, *519*, 42.
- (2) Yoon, T. P.; Ischay, M. A.; Du, J. *Nat. Chem.* **2010**, *2*, 527.

- (3) Narayanam, J. M. R.; Stephenson, C. R. J. *Chem. Soc. Rev.* **2011**, *40*, 102.
- (4) Maeda, K.; Sahara, G.; Eguchi, M.; Ishitani, O. *ACS Catal.* **2015**, *5*, 1700.
- (5) Kuriki, R.; Matsunaga, H.; Nakashima, T.; Wada, K.; Yamakata, A.; Ishitani, O.; Maeda, K. *J. Am. Chem. Soc.* **2016**, *138*, 5159.
- (6) Cuthbertson, J. D.; MacMillan, D. W. C. *Nature* **2015**, *519*, 74.
- (7) Jin, J.; MacMillan, D. W. C. *Nature* **2015**, *525*, 87.
- (8) Zuo, Z.; Ahneman, D. T.; Chu, L.; Terrett, J. A.; Doyle, A. G.; MacMillan, D. W. C. *Science* **2014**, *345*, 437.
- (9) Tellis, J. C.; Primer, D. N.; Molander, G. A. *Science* **2014**, *345*, 433.
- (10) Shu, X.-z.; Zhang, M.; He, Y.; Frei, H.; Toste, F. D. *J. Am. Chem. Soc.* **2014**, *136*, 5844.
- (11) Sahoo, B.; Hopkinson, M. N.; Glorius, F. *J. Am. Chem. Soc.* **2013**, *135*, 5505.
- (12) Hopkinson, M. N.; Sahoo, B.; Li, J.-L.; Glorius, F. *Chem. Eur. J.* **2014**, *20*, 3874.
- (13) Prier, C. K.; Rankic, D. A.; MacMillan, D. W. C. *Chem. Rev.* **2013**, *113*, 5322.
- (14) Vila, C. *ChemCatChem* **2015**, *7*, 1790.
- (15) Xie, J.; Shi, S.; Zhang, T.; Mehrkens, N.; Rudolph, M.; Hashmi, A. S. *Angew. Chem. Int. Ed. Engl.* **2015**, *54*, 6046.
- (16) Noble, A.; McCarver, S. J.; MacMillan, D. W. *J. Am. Chem. Soc.* **2015**, *137*, 624.
- (17) Primer, D. N.; Karakaya, I.; Tellis, J. C.; Molander, G. A. *J. Am. Chem. Soc.* **2015**, *137*, 2195.
- (18) Wang, F.; Li, C.; Chen, H.; Jiang, R.; Sun, L. D.; Li, Q.; Wang, J.; Yu, J. C.; Yan, C. H. *J. Am. Chem. Soc.* **2013**, *135*, 5588.
- (19) Chu, L.; Lipshultz, J. M.; MacMillan, D. W. *Angew. Chem. Int. Ed. Engl.* **2015**, *54*, 7929.
- (20) Higashimoto, S.; Kitao, N.; Yoshida, N.; Sakura, T.; Azuma, M.; Ohue, H.; Sakata, Y. *J. Catal.* **2009**, *266*, 279.
- (21) Ohkubo, K.; Suga, K.; Fukuzumi, S. *Chem. Commun.* **2006**, 2018.
- (22) Tanaka, A.; Hashimoto, K.; Kominami, H. *J. Am. Chem. Soc.* **2012**, *134*, 14526.
- (23) Chen, L.; Peng, Y.; Wang, H.; Gu, Z.; Duan, C. *Chem. Commun.* **2014**, *50*, 8651.
- (24) Lang, X.; Leow, W. R.; Zhao, J.; Chen, X. *Chem. Sci.* **2015**, *6*, 1075.
- (25) Lang, X.; Zhao, J.; Chen, X. *Angew. Chem. Int. Ed.* **2016**, *55*, 4697.
- (26) Zhang, M.; Chen, C.; Ma, W.; Zhao, J. *Angew. Chem. Int. Ed. Engl.* **2008**, *47*, 9730.
- (27) Sun, M.; Zhang, J.; Putaj, P.; Caps, V.; Lefebvre, F.; Pelletier, J.; Basset, J.-M. *Chem. Rev.* **2014**, *114*, 981.
- (28) Beller, M. *Adv. Synth. Catal.* **2004**, *346*, 107.
- (29) Langeron, M.; Fleury, M. B. *Science* **2013**, *339*, 43.
- (30) Langeron, M.; Fleury, M. B. *Angew. Chem. Int. Ed. Engl.* **2012**, *51*, 5409.
- (31) Lang, X.; Chen, X.; Zhao, J. *Chem. Soc. Rev.* **2014**, *43*, 473.
- (32) Shishido, T.; Miyatake, T.; Teramura, K.; Hitomi, Y.; Yamashita, H.; Tanaka, T. *J. Phys. Chem. C* **2009**, *113*, 18713.
- (33) Nagib, D. A.; Scott, M. E.; MacMillan, D. W. C. *J. Am. Chem. Soc.* **2009**, *131*, 10875.
- (34) Stevenson, S. M.; Shores, M. P.; Ferreira, E. M. *Angew. Chem. Int. Ed. Engl.* **2015**, *54*, 6506.
- (35) Cano-Yelo, H.; Deronzier, A. *Tetrahedron Lett.* **1984**, *25*, 5517.
- (36) Kim, W.; Tachikawa, T.; Majima, T.; Choi, W. *J. Phys. Chem. C* **2009**, *113*, 10603.
- (37) Canlas, C. P.; Lu, J.; Ray, N. A.; Grosso-Giordano, N. A.; Lee, S.; Elam, J. W.; Winans, R. E.; Van Duyne, R. P.; Stair, P. C.; Notestein, J. M. *Nat. Chem.* **2012**, *4*, 1030.
- (38) Ealet, B.; Elyakhloufi, M. H.; Gillet, E.; Ricci, M. *Thin Solid Films* **1994**, *250*, 92.
- (39) Shimizu, K.-i.; Sugino, K.; Sawabe, K.; Satsuma, A. *Chem. Eur. J.* **2009**, *15*, 2341.
- (40) Trueba, M.; Trasatti, S. P. *Eur. J. Inorg. Chem.* **2005**, *2005*, 3393.
- (41) Torres Galvis, H. M.; Bitter, J. H.; Khare, C. B.; Ruitenbeek, M.; Dugulan, A. I.; de Jong, K. P. *Science* **2012**, *335*, 835.
- (42) Lu, J.; Fu, B.; Kung, M. C.; Xiao, G.; Elam, J. W.; Kung, H. H.; Stair, P. C. *Science* **2012**, *335*, 1205.
- (43) Korhonen, S. T.; Beale, A. M.; Newton, M. A.; Weckhuysen, B. M. *J. Phys. Chem. C* **2011**, *115*, 885.
- (44) Thibault-Starzyk, F.; Seguin, E.; Thomas, S.; Daturi, M.; Arnolds, H.; King, D. A. *Science* **2009**, *324*, 1048.
- (45) Teramura, K.; Tanaka, T.; Yamamoto, T.; Funabiki, T. *J. Mol. Catal. A: Chem.* **2001**, *165*, 299.
- (46) Digne, M.; Sauteta, P.; Raybaud, P.; Euzenc, P.; Toulhoat, H. *J. Catal.* **2004**, *226*, 54.
- (47) Kresse, G.; Furthmüller, J. *Phys. Rev. B* **1996**, *54*, 11169.
- (48) Kresse, G.; Furthmüller, J. *Comput. Mater. Sci.* **1996**, *6*, 15.
- (49) Kresse, G.; Hafner, J. *Phys. Rev. B* **1993**, *47*, 558.
- (50) Kresse, G.; Hafner, J. *Phys. Rev. B* **1994**, *49*, 14251.
- (51) Blöchl, P. E. *Phys. Rev. B* **1994**, *50*, 17953.
- (52) Kresse, G.; Joubert, D. *Phys. Rev. B* **1999**, *59*, 1758.
- (53) Perdew, J. P.; Burke, K.; Ernzerhof, M. *Phys. Rev. Lett.* **1996**, *77*, 3865.
- (54) Wang, Q.; Zhang, M.; Chen, C.; Ma, W.; Zhao, J. *Angew. Chem. Int. Ed. Engl.* **2010**, *49*, 7976.
- (55) Liang, S.; Wen, L.; Lin, S.; Bi, J.; Feng, P.; Fu, X.; Wu, L. *Angew. Chem. Int. Ed. Engl.* **2014**, *53*, 2951.
- (56) Zhang, M.; Wang, Q.; Chen, C.; Zang, L.; Ma, W.; Zhao, J. *Angew. Chem. Int. Ed. Engl.* **2009**, *48*, 6081.
- (57) Suh, M.; Bagus, P. S.; Pak, S.; Rosynek, M. P.; Lunsford, J. H. *J. Phys. Chem. B* **2000**, *104*, 2736.
- (58) Asbury, J. B.; Ellingson, R. J.; Ghosh, H. N.; Ferrere, S.; Nozik, A. J.; Lian, T. *J. Phys. Chem. B* **1999**, *103*, 3110.
- (59) Riener, M.; Nicewicz, D. A. *Chem. Sci.* **2013**, *4*, 2625.
- (60) Zhang, J.; Chen, J.; Zhang, X.; Lei, X. *J. Org. Chem.* **2014**, *79*, 10682.
- (61) Kranz, D. P.; Griesbeck, A. G.; Alle, R.; Perez-Ruiz, R.; Neudörfl, J. M.; Meerholz, K.; Schmalz, H.-G. *Angew. Chem. Int. Ed.* **2012**, *51*, 6000.
- (62) Flockhart, B. D.; Scott, J. A. N.; Pink, R. C. *J. Chem. Soc. Faraday Trans.* **1966**, *62*, 730.
- (63) Li, F. T.; Liu, S. J.; Xue, Y. B.; Wang, X. J.; Hao, Y. J.; Zhao, J.; Liu, R. H.; Zhao, D. *Chem. Eur. J.* **2015**, *21*, 10149.
- (64) Lee, M. M.; Teuscher, J.; Miyasaka, T.; Murakami, T. N.; Snaith, H. J. *Science* **2012**, *338*, 643.
- (65) Carnie, M. J.; Charbonneau, C.; Davies, M. L.; Troughton, J.; Watson, T. M.; Wojciechowski, K.; Snaith, H.; Worsley, D. A. *Chem. Commun.* **2013**, *49*, 7893.

Table of Contents

We discovered that the oxidation potentials of benzyl alcohols and O₂ can be reduced through surface complexation with Al₂O₃, thereby allowing its photocatalytic transformation in the presence of different dyes.

